Available online at www.sciencedirect.com
ScienceDirect
Physica E 40 (2007) 103–110
PHYSICA E
www.elsevier.com/locate/physe

Noise measurements in quantum dots using charge detection techniques

S. Gustavsson[a], R. Leturcq[a], T. Ihn[a], K. Ensslin[a,*], D.C. Driscoll[b], A.C. Gossard[b]

[a]*Solid State Physics Laboratory, ETH Zürich, HPF E 3 Schafmattstr. 16 CH-8093 Zürich, Switzerland*
[b]*Materials Department, University of California, Santa Barbara, CA 93106, USA*

Available online 29 May 2007

Abstract

We have measured the current fluctuations in a quantum dot using a quantum point contact as a charge detector. By determining the distribution function for the charge transferred through the quantum dot, we get access not only to the shot noise but also to higher order moments. The noise in the quantum dot was found to be reduced compared to the single-barrier case. The reduction can be explained by an increase in temporal correlation due to the Coulomb blockade. Furthermore, we have used the time-resolved measurement techniques to investigate degenerate states in the quantum dot.

PACS: 72.70.+m; 73.23.Hk; 73.63.Kv

Keywords: Quantum dots; Noise measurements; Coulomb blockade

1. Introduction

Temporal current fluctuations in conductors have been intensely investigated due to the additional information they provide compared to the average current, in particular for interacting systems [1]. Shot noise measurements demonstrated the charge of quasi-particles in the fractional quantum Hall effect [2,3] and in superconductors [4].

For independent particles tunneling through a single barrier, the current fluctuations are expected to follow a Poisson distribution. In electron transport through a semiconductor quantum dot (QD), the noise is typically suppressed compared to the Poisson distribution, giving sub-Poissonian noise. This is due to the Coulomb blockade, which enhances the temporal correlation between electrons and thereby reduces the noise [5]. However, when several channels with different coupling strengths contribute to electron transport, interactions can lead to more complex processes and to an enhancement of the noise [6–9]. Furthermore, there are predictions that entangled electrons may lead to super-Poissonian noise, thus making noise measurements a possible way of detecting entanglement in mesoscopic systems [10,11].

The suppression of shot noise due to Coulomb blockade has been detected in vertical QDs [12–14]. For lateral QDs, conventional measurement techniques are difficult to use due to the very low current levels involved. Recent attempts include using a resonant circuit together with a low-temperature amplifier [15,16], a superconductor–insulator–superconductor junction [17] or a second QD acting as a high-frequency detector [18].

A different approach is to use time-resolved charge detection methods to count the electrons one-by-one as they pass through the conductor. From such a measurement, one can directly determine the probability distribution function $p_{t_0}(N)$. The distribution gives the probability that N electrons are transferred through the conductor within a time interval of length t_0. The distribution function can then be used to calculate both the shot noise as well as higher order correlations. This way of measuring is analogous to the theoretical concept of full counting statistics (FCS), which was introduced as a new way of examining current fluctuations [19].

A difficulty with the experimental method is that it requires a very sensitive, non-invasive, high-bandwidth charge detector, capable of resolving individual electrons.

*Corresponding author. Tel.: +41 1 633 2209; fax: +41 44 633 11 46.
E-mail address: ensslin@phys.ethz.ch (K. Ensslin).

1386-9477/$ - see front matter © 2007 Elsevier B.V. All rights reserved.
doi:10.1016/j.physe.2007.05.018

Examples of devices fulfilling these requirements include the single electron transistor [20–22] and the quantum point contact (QPC) [23–25]. Using charge detection techniques, the noise and higher order moments of the current distribution have been measured in both a single QD [9,26,27] and a double QD [28]. Here, we summarize the results of previous work [26] and present further results from measurements involving time-resolved charge detection techniques.

2. Experimental setup

The QD used in the experiment is shown in Fig. 1(a). The structure was fabricated using scanning probe lithography [29] on a GaAs/$Al_{0.3}Ga_{0.7}As$ heterostructure with a two-dimensional electron gas (2DEG) 34 nm below the surface. The sample consists of a QD [dotted circle in Fig. 1(a)] and a nearby QPC. The charging energy of the QD is 2.1 MeV and the mean level spacing is 200–300 μeV. From the geometry and the characteristic energy scales, we estimate that the QD contains about 30 electrons. The QD is connected to the source and drain leads through tunnel barriers. The transparency of the tunnel barriers can be controlled by changing the voltage on gates $G1$ and $G2$. In this experiment, the tunnel coupling strengths between the QD and the leads were reduced to below 10 kHz. The P gate was used to tune the conductance of the QPC to a regime where the sensitivity to changes in the dot charge is maximal. Due to a resonance in the QPC, we chose not to operate the QPC at the usual operating point half-way below the first conductance plateau, with $G_{QPC} = e^2/h$. Instead, the best sensitivity was reached at $G_{QPC} \sim 0.25\, e^2/h$. The conductance was measured by voltage biasing the QPC ($V_{bias} = 500\,\mu V$) and reading out the current. Because of the capacitive coupling between gates $G1$, $G2$ and the QPC, the voltage on gate P had to be adjusted to keep the QPC in the region of maximum sensitivity whenever a voltage on the other gates was changed. The bandwidth of the QPC circuit was 30 kHz. All measurements were performed in a dilution refrigerator with a base temperature of 60 mK.

3. Extracting the tunneling rates

In the low-bias regime, the QD can only hold one excess electron. Before a second electron can enter, the first one has to go out. When an electron enters the QD, the conductance through the QPC is reduced due to the electrostatic coupling between the QD and the QPC. As the electron leaves, the QPC conductance returns to the original value. This gives rise to a QPC current switching between two levels, as shown in Fig. 1(b). The low level corresponds to a situation where the dot holds an excess electron. Transitions between the two levels occur whenever an electron enters or leaves the QD. The time between

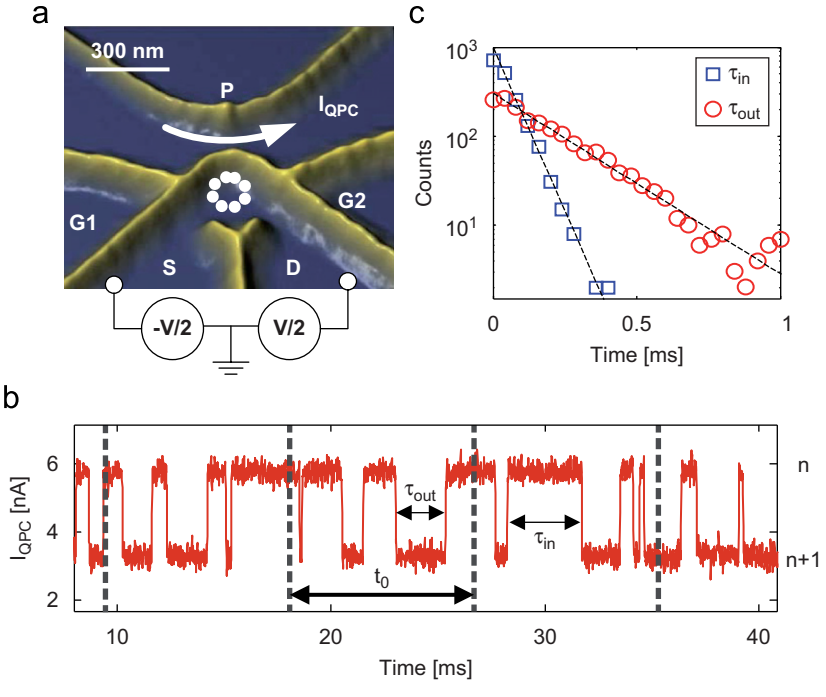

Fig. 1. (a) Quantum dot with integrated charge read-out used in the experiment. (b) Current through the QPC as a function of time, showing a few electrons tunneling into and out of the QD. The lower current level corresponds to a situation where the QD contains one excess electron. Transitions between the two levels occur whenever an electron enters or leaves the QD. The quantities τ_{in} and τ_{out} specify the time it takes for an electron to tunnel into and out of the dot, respectively. (c) Distribution of tunneling times for electrons entering (squares) and leaving (circles) the dot. The solid lines show the exponential behavior given by Eq. (2) in the text, with $\Gamma_{in} = 1/\langle\tau_{in}\rangle = 7.3$ kHz, $\Gamma_{out} = 1/\langle\tau_{out}\rangle = 2.0$ kHz. The length of the time trace for the data shown in the figure is 0.5 s.

the transitions give the time it takes for an electron to tunnel into or out of the QD. In Fig. 1(b), these times are marked by τ_{in}, τ_{out}.

In the regime of single-level transport, the process of an electron tunneling into or out of the dot is described by the rate equation

$$\dot{p}_{in/out}(t) = -\Gamma_{in/out} p_{in/out}(t). \quad (1)$$

Here, $p_{in/out}(t)$ is the probability density for an electron to tunnel into or out of the dot at a time t after a complementary event. Solving the differential equation and normalizing the resulting distribution gives

$$p_{in/out}(t)\,dt = \Gamma_{in/out} e^{-\Gamma_{in/out} t}\,dt. \quad (2)$$

Eq. (2) is valid assuming non-degenerate states. In the case of degenerate states, the rates should be multiplied with the appropriate degeneracy factor. Here, we assume non-degenerate states and postpone the discussion of degenerate states to Section 6.

The experimental distribution function $p_{in/out}(t)$ can be determined by extracting the tunneling times τ_{in}, τ_{out} from a time trace containing a large number of events. Such a distribution is shown in Fig. 1(c), taken from a trace of length $T = 0.5$ s. The data show the expected exponential behavior of Eq. (2), the black dashed lines are fits with $\Gamma_{in} = 7.3$ kHz and $\Gamma_{out} = 2.0$ kHz.

Even though the probability distribution shown in Fig. 1(c) seems to follow the result of Eq. (2), it should be noted that the finite bandwidth of the detector introduces systematic changes in the measured distribution [30]. The very fast tunneling events are less likely to be detected, giving a cut-off for short time scales in the measured distribution. Moreover, since the fast events are not detected, the measurement will over-estimate the occurrence of slow events. The long-time tail of the measured distribution will still decay exponentially, but the tunneling rate extracted from a distribution such as the one shown in Fig. 1(c) will be under-estimated. However, the true tunneling rates can still be retrieved by compensating for the finite bandwidth. The compensations are given as [30]

$$\Gamma_{in} = \Gamma^*_{in} \frac{(\Gamma_{det} - \Gamma^*_{out})(\Gamma_{det} - \Gamma^*_{in} + \Gamma^*_{out})}{\Gamma_{det}(\Gamma_{det} - \Gamma^*_{in} - \Gamma^*_{out})}, \quad (3)$$

$$\Gamma_{out} = \Gamma^*_{out} \frac{(\Gamma_{det} - \Gamma^*_{in})(\Gamma_{det} + \Gamma^*_{in} - \Gamma^*_{out})}{\Gamma_{det}(\Gamma_{det} - \Gamma^*_{in} - \Gamma^*_{out})}. \quad (4)$$

Here, $\Gamma_{in/out}$ are the true tunneling rates, $\Gamma^*_{in/out}$ are the detected rates and Γ^*_{det} is the rate of the detector. The maximal detection rate Γ_{det} is essentially the rise time of the detector, it depends not only on the measurement bandwidth but also on the signal-to-noise ratio of the detector signal as well as the redundancy needed to minimize the risk of detecting false events [31]. Using Eqs. (3), (4) with a maximal detection rate of $\Gamma_{det} = 100$ kHz, we find that the true tunneling rates for the data presented in Fig. 1(c) are $\Gamma_{in} = 7.5$ kHz and $\Gamma_{out} = 2.2$ kHz.

4. Measuring the current statistics

To use the charge detector for measuring current, one has to avoid that electrons tunnel back and forth between the dot and the source or drain lead due to thermal fluctuations [Fig. 2(a)]. This is achieved by applying a finite bias voltage between source and drain, i.e. $k_B T \ll |\pm eV/2 - E_d| \ll E_C$, where E_C is the charging energy, E_d is the electrochemical potential of the dot and V is the bias voltage, symmetrically applied to the QD [Fig. 2(b)]. With a finite bias applied to the QD, and with the Fermi levels of the leads far away from the electrochemical potential of the QD, the probability for electrons to tunnel in the opposite direction is exponentially suppressed. In this regime, we can attribute each transition $n \to n+1$ to an electron entering the QD from the source contact, and each transition $n+1 \to n$ to an electron leaving the QD to the drain contact. The charge fluctuations in the QD correspond to a non-equilibrium process, and are directly related to the current through the dot. This makes it possible to measure the current by counting the electrons traveling through the system.

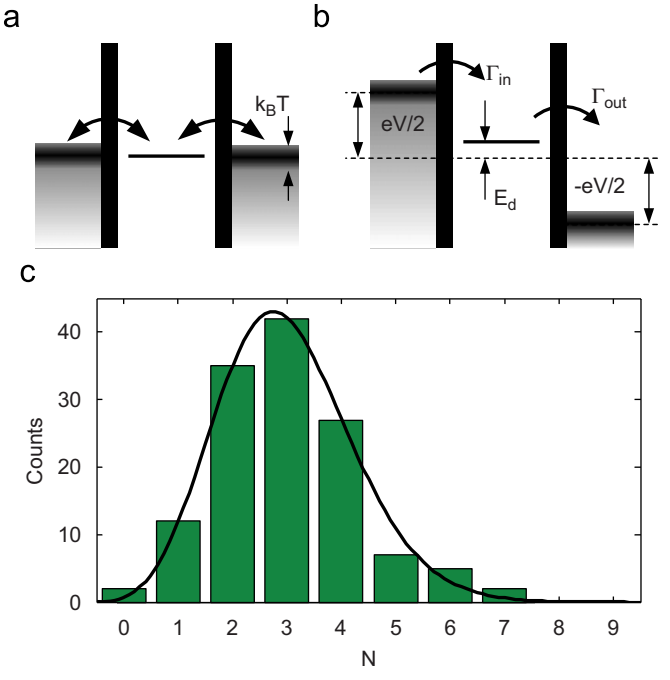

Fig. 2. (a) Energy level diagram for the quantum dot in the regime of equilibrium fluctuations. Electrons may leave or enter the dot from either of the two leads. (b) Energy level diagram for the quantum in the high-bias regime. With a large bias applied to the QD, and with the Fermi levels of the leads far away from the electrochemical potential of the dot, electrons can only enter the QD from the source lead and only leave to the drain. (c) Current distribution function $p_{t_0}(N)$, determined from a trace of data similar to the one shown in Fig. 1(b). The time t_0 was chosen so that $\langle N \rangle = 3$. The solid line shows the result of Eqs. (11), (12) in the text, with $\Gamma_{in} = 1.7$ kHz and $\Gamma_{out} = 1.4$ kHz.

In the finite bias regime, the tunneling rates $\Gamma_{\rm in}$ and $\Gamma_{\rm out}$ give directly the current

$$I = e\frac{\Gamma_{\rm in}\Gamma_{\rm out}}{\Gamma_{\rm in}+\Gamma_{\rm out}}. \quad (5)$$

From the tunneling rates, one could calculate all the higher moments of the current distribution as well. However, the results are only valid assuming that Eq. (2) is correct. In order to measure the current and the current distribution function for *any* experimental configuration, we instead focus on determining the current distribution function $p_{t_0}(N)$ directly from the experimental data.

The distribution $p_{t_0}(N)$ describes the probability that N electrons are transferred through the conductor within a time t_0. The distribution is formed by splitting a time trace of length T into $m = T/t_0$ intervals of length t_0 and counting the number of electrons entering the QD within each interval. An example of such a distribution is shown in Fig. 2(c). The noise and the higher moments can then be calculated directly from the measured distribution function. The second moment $[\mu_2 = \langle N^2\rangle - \langle N\rangle^2]$ describe the variance or the width of the distribution, while the third moment $[\mu_3 = (N - \langle N\rangle)^3]$ is a measure of its asymmetry.

A complication of the method is the finite length of each time trace. In the experiment, it is favorable to make t_0 as short as possible in order to increase the number of samples $m = T/t_0$. This will improve the quality of the distribution and help to minimize statistical errors. On the other hand, making t_0 too short will alter the distribution and may diminish the influence of long-time correlations in the measured noise. It is therefore important to carefully check the influence of the interval length t_0 when analyzing the data [27].

Another limitation of the method is that the finite bandwidth of the detector will alter the measured statistics. The effect is similar to the corrections introduced when determining the tunneling rates, as described in Section 3. The finite bandwidth makes it less probable for the detector to detect fast events, meaning that the probability of detecting a large number of electrons within an interval t_0 will decrease more than the probability of detecting few electrons. This will cut the high-count tail of the distribution and thereby reduce both the width and the asymmetry. The problem can be circumvented by including the detector into the model of the system and calculating the noise for the combined detector-QD system [27]. With the limitations of the detector incorporated into the system, it is possible to calculate the influence of the finite bandwidth on the measured statistics.

5. Current noise in a single-level QD

To illuminate the principle of operation of our device, we investigate the noise of the QD in the sequential tunneling regime. The FCS of electron transport in a QD in this regime has been calculated before [32]. Here, we summarize the theory, we apply the conditions appropriate for our experimental configuration and at the end we compare the results with the experimental data.

5.1. Theory and model description

We model the occupancy of the QD in the low-bias regime by the rate equation

$$\frac{\rm d}{{\rm d}t}\begin{pmatrix} p_n \\ p_{n+1}\end{pmatrix} = \begin{pmatrix} -\Gamma_{\rm in} & \Gamma_{\rm out} \\ \Gamma_{\rm in} & -\Gamma_{\rm out}\end{pmatrix}\begin{pmatrix} p_n \\ p_{n+1}\end{pmatrix}. \quad (6)$$

Here, p_n and p_{n+1} give the occupation probability for the states with n and $n+1$ electrons, respectively. The tunneling rates are given by

$$\Gamma_{\rm in} = \Gamma_{\rm L} f_{\rm L}(E_{\rm d}) + \Gamma_{\rm R} f_{\rm R}(E_{\rm d}), \quad (7)$$

$$\Gamma_{\rm out} = \Gamma_{\rm L}[1 - f_{\rm L}(E_{\rm d})] + \Gamma_{\rm R}[1 - f_{\rm R}(E_{\rm d})], \quad (8)$$

where $f_{\rm L}$ and $f_{\rm R}$ are the Fermi distributions in the left and right leads and $E_{\rm d}$ is the electrochemical potential of the QD. Eqs. (7), (8) are valid assuming non-degenerate states, the case of degenerate states is discussed in Section 6.

These rates can be simplified in the case of large bias voltage, $|\pm eV/2 - E_{\rm d}| \gg k_{\rm B}T$. Here, electrons can only tunnel into the QD through one lead, the source (being either left or right lead, depending on the sign of the bias voltage), and can only tunnel out of the QD through the other contact, the drain. With positive (negative) bias, we have $f_{\rm L(R)}(E_{\rm d}) = 1$ and $f_{\rm R(L)}(E_{\rm d}) = 0$. This gives

$$\Gamma_{\rm in} = \Gamma_{\rm L(R)} = \Gamma_{\rm S} \quad \text{and} \quad \Gamma_{\rm out} = \Gamma_{\rm R(L)} = \Gamma_{\rm D}. \quad (9)$$

In this model, $\Gamma_{\rm S}$ and $\Gamma_{\rm D}$ are assumed to be independent of energy. The model can be extended to the transport through multiple states in the QD. The effective tunneling rates will be the sum of the individual tunneling rates for all the involved states.

To perform the counting statistics, we need to introduce a counting field $e^{i\chi}$ in the rate equation. In our case, we count electrons tunneling into the QD, and the matrix from Eq. (6) can be written as

$$M(\chi) = \begin{pmatrix} -\Gamma_{\rm in} & \Gamma_{\rm out} \\ \Gamma_{\rm in} * e^{i\chi} & -\Gamma_{\rm out}\end{pmatrix}. \quad (10)$$

The distribution function for the number of electrons tunneling through the QD during a time t_0 can be generated from the cumulant-generating function $S(\chi)$:

$$p_{t_0}(N) = \int_{-\pi}^{\pi}\frac{{\rm d}\chi}{2\pi}e^{-S(\chi)-iN\chi}. \quad (11)$$

In the limit $t_0 \gg \Gamma_{\rm in}^{-1}, \Gamma_{\rm out}^{-1}$, the normalized distribution $p_{t_0}(N/t_0)$ is independent of t_0. In the same limit, the cumulating-generating function $S(\chi)$ is related to the lowest eigenvalue of $M(\chi)$, $\lambda_0(\chi)$ as

$$S(\chi) = \lambda_0(\chi)t_0 = \frac{t_0}{2}\left[\Gamma_{\rm in}+\Gamma_{\rm out} - \sqrt{(\Gamma_{\rm in}-\Gamma_{\rm out})^2 + 4\Gamma_{\rm in}\Gamma_{\rm out}e^{-i\chi}}\right]. \quad (12)$$

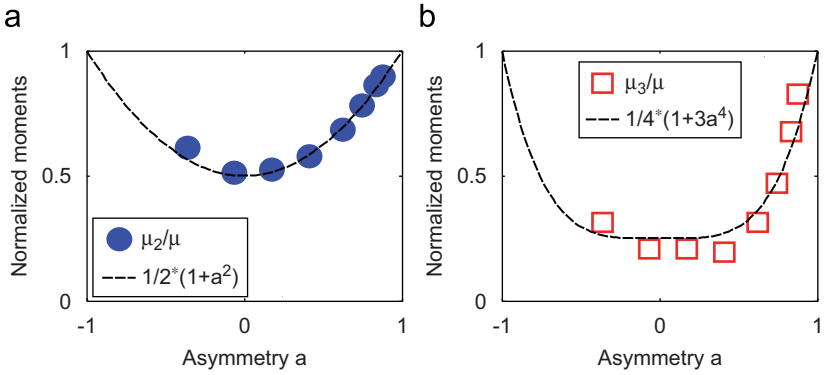

Fig. 3. Normalized moments versus asymmetry of the tunnel coupling, $a = (\Gamma_{in} - \Gamma_{out})/(\Gamma_{in} + \Gamma_{out})$. The dashed lines are theoretical predictions for the two-state model described in the text.

Knowing the distribution function $p_{t_0}(N)$, one can calculate all moments characterizing the current fluctuations. In the following we are interested in the three first central moments μ_i, which coincide with the first three cumulants C_i. These can then be generated directly from the cumulant-generating function $S(\chi)$. The mean current is given by the first cumulant C_1 of the distribution:

$$I = \frac{e}{t_0} C_1 = \frac{e}{t_0} \left(-\mathrm{i} \frac{\mathrm{d}S}{\mathrm{d}\chi} \right)_{\chi=0} = e \frac{\Gamma_{in}\Gamma_{out}}{\Gamma_{in} + \Gamma_{out}} \ . \tag{13}$$

The symmetrized shot noise is given by the variance, or the second cumulant C_2, of the distribution:

$$S_I = \frac{2e^2}{t_0} C_2 = \frac{2e^2}{t_0} \left(-\frac{\mathrm{d}^2 S}{\mathrm{d}\chi^2} \right)_{\chi=0}, \tag{14}$$

from which we can calculate the Fano factor:

$$F_2 = \frac{S_I}{2eI} = \frac{C_2}{C_1} = \frac{\Gamma_{in}^2 + \Gamma_{out}^2}{(\Gamma_{in} + \Gamma_{out})^2} = \frac{1}{2}(1 + a^2), \tag{15}$$

where $a = (\Gamma_{in} - \Gamma_{out})/(\Gamma_{in} + \Gamma_{out})$ is the asymmetry of the coupling. This result recovers the earlier calculations for the shot noise in a QD [5], and shows the reduction of the noise by a factor $\frac{1}{2}$ for a QD symmetrically coupled to the leads, while the Poissonian limit, $F_2 = 1$, is reached for an asymmetrically coupled QD.

Finally, we are also interested in the third central moment, or third cumulant C_3, of the fluctuations, which characterizes the asymmetry of the distribution (skewness):

$$C_3 = \mathrm{i} \left(\frac{\mathrm{d}^3 S}{\mathrm{d}\chi^3} \right)_{\chi=0}. \tag{16}$$

The asymmetry can also be normalized to the mean of the distribution:

$$F_3 = \frac{C_3}{C_1} = \frac{\Gamma_{in}^4 - 2\Gamma_{in}^3\Gamma_{out} + 6\Gamma_{in}^2\Gamma_{out}^2 - 2\Gamma_{in}\Gamma_{out}^3 + \Gamma_{out}^4}{(\Gamma_{in} + \Gamma_{out})^4}$$
$$= \frac{1}{4}(1 + 3a^4). \tag{17}$$

The result shows that for a symmetrically coupled QD, the third moment is reduced by a factor $\frac{1}{4}$ compared to the Poissonian limit. For an asymmetrically coupled dot with $a \to \pm 1$, we again retrieve $F_3 \to 1$.

5.2. Experimental results

Eqs. (15), (17) express the expected noise as a function of the asymmetry of the tunneling rates. In the experiment, the tunnel couplings can be tuned by changing the voltages on gates $G1$ and $G2$. Figure 3 shows the measured second and third moments, determined at eight different gate voltage configurations. Both the moments and the asymmetry of each configuration were extracted directly from the measured time traces. The moments were evaluated as described in Section 4, while the asymmetry was given by the tunneling rates, extracted using the methods of Section 3.

The figure shows a reduction of the noise for a symmetrically coupled QD compared to the values $\mu_2/\mu = \mu_3/\mu = 1$ expected for a single barrier. This is due to Coulomb blockade; a second electron cannot enter the dot before the first one leaves. The effect increases the correlations between tunneling electrons and thereby reduces the noise. As the tunnel couplings of the barriers grow more asymmetric, the transport is essentially governed by the weakly transparent barrier and the noise approaches the single-barrier value.

The dashed lines in Fig. 3 are the theoretical prediction for the moment, given in Eqs. (15),(17). The figure shows good agreement between the experimental data and the theoretical predictions, especially considering that the model does not involve any free parameters. The precision of the measurement can be enhanced by increasing the length of each time trace, with the limiting factor being the stability of the sample. It should be noted that the method can in principle be used to extract cumulants of any order; again, the limiting factor being the amount of data available. In another set of measurement, using traces of length $T = 10$ min, we were able to determine the first five cumulants [27].

6. Degenerate states

In this section, we discuss how degenerate states may influence the measured statistics. For simplicity, we limit the discussion to the case where the QD is connected only to one lead, with the other lead being completely pinched off. In this configuration, the tunneling is due to equilibrium fluctuations between the QD and the lead. Fig. 4(a) shows the average DC current through the QPC when sweeping the two gates $G1$ and $G2$. The diagonal lines correspond to electrons being loaded/unloaded from the QD. Along those lines, the electrochemical potential of the QD is aligned with the Fermi level of the lead. From the slope of the line we see that the voltages on the two gates $G1$ and $G2$ have roughly the same influence on the energy levels of the QD, as expected from the device geometry. We now focus on determining the tunneling rates for three electronic states along the dotted line in Fig. 4(a). Starting at low V_{G1} voltages, the dot gets successively populated as the voltage on $G1$ is increased. At each charge degeneracy point, we use the time-resolved measurement techniques to determine the rates for electrons entering and leaving the dot. The results are shown in Fig. 4(b).

In the single-lead case, the results of Eqs. (7), (8) simplify to

$$\Gamma_{\rm in} = g_{\rm in}\,\Gamma_{\rm R} f_{\rm R}(E_{\rm d}), \tag{18}$$

$$\Gamma_{\rm out} = g_{\rm out}\,\Gamma_{\rm R}[1 - f_{\rm R}(E_{\rm d})]. \tag{19}$$

Here, we have included the factors $g_{\rm in}$ and $g_{\rm out}$ to account for possible degeneracies in a very simple model. For electrons entering the QD, the factor $g_{\rm in}$ should include the number of degenerate *empty* states. For tunneling out, only the degeneracy of *occupied* states is relevant. The tunnel coupling $\Gamma_{\rm R}$ is assumed to be independent of energy and of the QD level within the small gate voltage range considered here. The energy level for three different gate voltages are drawn schematically in Fig. 4(c). The middle plot of Fig. 4(b) indicates the gate voltage ranges corresponding to the drawings shown in Fig. 4(c).

The effective rates for electrons tunneling into and out of the QD involve the density of states and the occupation probability in the lead. This gives a strong dependence on the alignment between the Fermi level in the lead and the electrochemical potential of the dot. Starting at low V_{G1} voltages in Fig. 4(b) [case I in Fig. 4(c)], the QD potential is

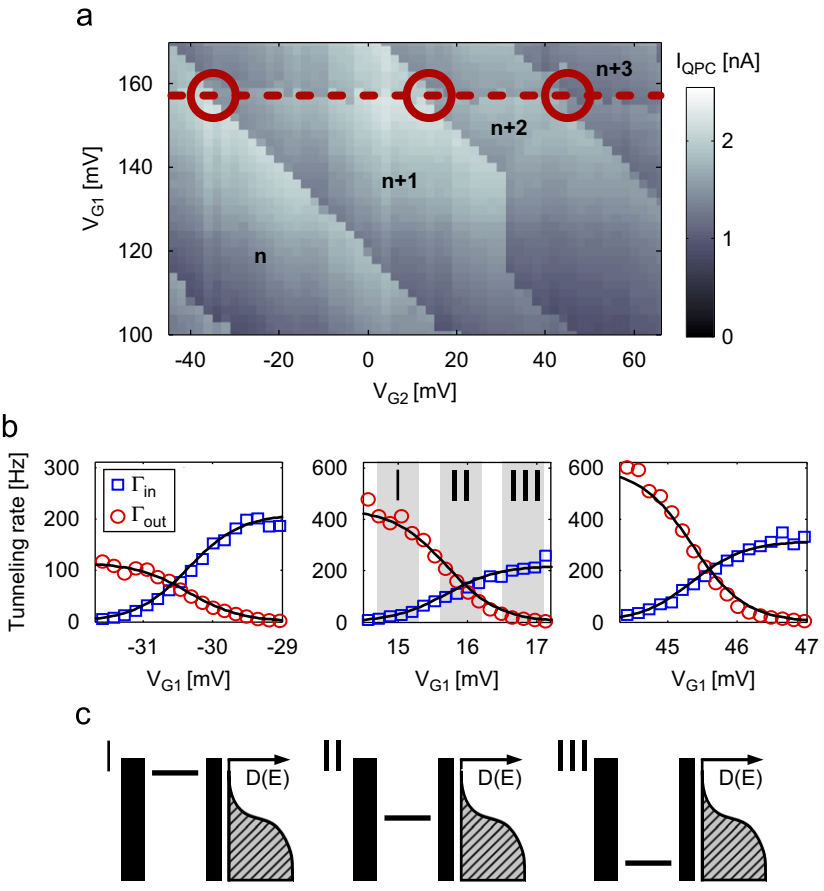

Fig. 4. (a) Current through the QPC as a function of voltage on gates $G1$, $G2$. The diagonal lines show positions where the charge of the QD changes by one electron. The numbers specify the dot occupation in the different regions. (b) Effective tunneling rates for electrons entering and leaving the dot, measured at the three charge degeneracy points marked by circles along the dashed line in (a). The solid lines are fits using Eqs. (18), (19), with $T = 230$ mK and the other fitting parameters given in Table 1 in the text. (c) Alignment of the QD electrochemical potential relative to the Fermi level of the lead for the gate voltage configurations shown in the middle plot in (b).

far above the Fermi level of the lead. At this point, the density of occupied states in the lead is low and the effective rate for tunneling into the QD is low. If an electron eventually manages to tunnel in, the effective rate for tunneling out again will be high, since there are many empty states in the lead to tunnel into. As the gate voltage is increased, the QD potential goes down to the Fermi level of the lead [case II in Fig. 4(b, c)]. In this configuration, the effective rates for tunneling into and out of the QD are roughly equal. As the gate voltage is further increased, the potential of the QD is pushed below the Fermi level. Here, the density of occupied states in the lead is large, giving a high effective rate for electrons entering the QD. Conversely, the effective rate for leaving the dot is low [case III in Fig. 4(b, c)].

Looking at the shape of the data in Fig. 4(b), we see that they indeed follow a Fermi function. The solid lines in the figure are fits using Eqs. (18), (19), with $T = 230\,\mathrm{mK}$. The lever arm between the gate voltage and the potential of the QD was determined in a standard Coulomb diamond measurement [33]. The parameters used in the fitting procedure are summarized in Table 1.

Comparing the numbers of Table 1, we see that the effective coupling $g_{\mathrm{in/out}}\,\Gamma_{\mathrm{R}}$ differs strongly depending on whether it was extracted from the tunneling in or from the tunneling out data. One possible explanation for the difference is degeneracy due to the electron spin. Assuming a spin-degenerate state with both the spin up and the spin down state initially empty, an electron could tunnel into either of the two states. This makes $g_{\mathrm{in}} = 2$. Once the electron has tunneled into the QD, it sits in either the spin up or the spin down state. Since only one of the spin-degenerate states is occupied, the degeneracy for tunneling out will be $g_{\mathrm{out}} = 1$. The situation is different if we start with a QD with one of the spin-degenerate states already occupied. For the tunneling-in process, there is only one empty state available, giving $g_{\mathrm{in}} = 1$. For the tunneling-out process, any of the two electrons sitting on the dot may tunnel out. This leads to $g_{\mathrm{out}} = 2$. The different situations are shown schematically in Fig. 5.

The tunnel couplings and spin degeneracies extracted from the data using this model are shown in Table 2. For the first resonance at $V_{G1} = -30.35\,\mathrm{mV}$, $g_{\mathrm{in}} = 2$ and $g_{\mathrm{out}} = 1$, indicating a spin degeneracy with both states initially empty. At the next resonance, the degeneracy factors are exchanged, with $g_{\mathrm{in}} = 1$ and $g_{\mathrm{out}} = 2$. For the third resonance, the degeneracy factors are the same as for the second resonance, with $g_{\mathrm{in}} = 1$ and $g_{\mathrm{out}} = 2$.

Table 1
Fitting parameters for the solid lines in Fig. 4(b), fitted using Eqs. (18), (19)

V_{G1} (mV)	$g_{\mathrm{in}}\,\Gamma_{\mathrm{R}}$ (Hz)	$g_{\mathrm{out}}\,\Gamma_{\mathrm{R}}$ (Hz)
−30.35	210	115
15.70	220	440
45.35	315	600

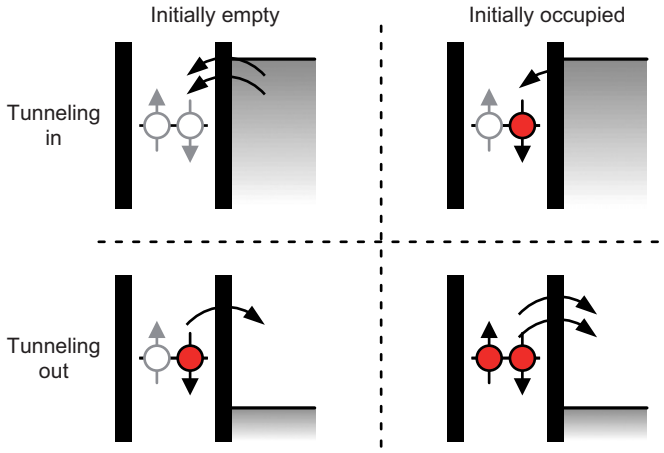

Fig. 5. Effective tunneling rates for spin-degenerate states in different configurations. The empty circles represent empty spin states, filled circles represent occupied ones. The arrows depict the number of possible tunnel processes.

Table 2
Interpretation of the data shown in Table 1, assuming spin-degenerate states

V_{G1} (mV)	Γ_{R} (Hz)	g_{in}	g_{out}
−30.35	110	2	1
15.70	220	1	2
45.35	307	1	2

The first and second resonance could be attributed to consecutive filling of the spin states, meaning that the two first electrons would be a so-called spin pair. The third electron does not follow the rules expected from simple spin-filling. The reason could be due to many-body effects between the electrons in the QD or due to a charge rearrangement taking place between the second and third resonance. Also, we stress that there are other possible explanations for the measurement results, like energy-dependent tunneling rates or accidental degeneracies of orbital states. To prove the spin degeneracy, one would need to perform measurements at non-zero magnetic fields. This would lift the spin degeneracy and make $g_{\mathrm{in}} = 1$ and $g_{\mathrm{out}} = 1$.

7. Conclusion

We have measured the time-resolved charge fluctuations in a QD using a QPC as a charge detector. In the large bias regime, where the electron motion is unidirectional and the charge fluctuations are directly related to the current fluctuations, we have extracted the distribution function for the charge transferred through the QD. From the distribution function, not only the mean current and shot noise, but also higher order moments can be extracted. We have also shown that the charge detection techniques can be used to investigate degenerate states in a QD.

References

[1] Y.M. Blanter, M. Buttiker, Phys. Rep. 336 (2000) 1.
[2] R. de Picciotto, M. Reznikov, M. Heiblum, V. Umansky, G. Bunin, D. Mahalu, Nature 389 (1997) 162.
[3] L. Saminadayar, D.C. Glattli, Y. Jin, B. Etienne, Phys. Rev. Lett. 79 (1997) 2526.
[4] X. Jehl, M. Sanquer, R. Calemczuk, D. Mailly, Nature 405 (2000) 50.
[5] J.H. Davies, P. Hyldgaard, S. Hershfield, J.W. Wilkins, Phys. Rev. B 46 (1992) 9620.
[6] E.V. Sukhorukov, G. Burkard, D. Loss, Phys. Rev. B 63 (2001) 125315.
[7] A. Cottet, W. Belzig, C. Bruder, Phys. Rev. B 70 (2004) 115315.
[8] W. Belzig, Phys. Rev. B 71 (2005) 161301 (R).
[9] S. Gustavsson, R. Leturcq, B. Simovic, R. Schleser, P. Studerus, T. Ihn, K. Ensslin, D.C. Driscoll, A.C. Gossard, Phys. Rev. B 74 (2006) 195305.
[10] D. Loss, E.V. Sukhorukov, Phys. Rev. Lett. 84 (2000) 1035.
[11] D.S. Saraga, D. Loss, Phys. Rev. Lett. 90 (2003) 166803.
[12] H. Birk, M.J.M. de Jong, C. Schönenberger, Phys. Rev. Lett. 75 (1995) 1610.
[13] A. Nauen, I. Hapke-Wurst, F. Hohls, U. Zeitler, R.J. Haug, K. Pierz, Phys. Rev. B 66 (2002) 161303 (R).
[14] A. Nauen, F. Hohls, N. Maire, K. Pierz, R.J. Haug, Phys. Rev. B 70 (2004) 033305.
[15] O. Zarchin, Y.C. Chung, M. Heiblum, V. Umansky, 2006, cond-mat/0607756.
[16] D.T. McClure, L. DiCarlo, Y. Zhang, H.A. Engel, C.M. Marcus, M.P. Hanson, A.C. Gossard, 2006, cond-mat/0607280.
[17] E. Onac, F. Balestro, B. Trauzettel, C.F.J. Lodewijk, L.P. Kouwenhoven, Phys. Rev. Lett. 96 (2006) 026803.
[18] E. Onac, F. Balestro, L.H.W. van Beveren, U. Hartmann, Y.V. Nazarov, L.P. Kouwenhoven, Phys. Rev. Lett. 96 (2006) 176601.
[19] L.S. Levitov, H.W. Lee, G.B. Lesovik, J. Math. Phys. 37 (1996) 4845.
[20] W. Lu, Z. Ji, L. Pfeiffer, K.W. West, A.J. Rimberg, Nature 423 (2003) 422.
[21] T. Fujisawa, T. Hayashi, Y. Hirayama, H.D. Cheong, Y.H. Jeong, Appl. Phys. Lett. 84 (2004) 2343.
[22] J. Bylander, T. Duty, P. Delsing, Nature 434 (2005) 361.
[23] M. Field, C.G. Smith, M. Pepper, D.A. Ritchie, J.E.F. Frost, G.A.C. Jones, D.G. Hasko, Phys. Rev. Lett. 70 (1993) 1311.
[24] R. Schleser, E. Ruh, T. Ihn, K. Ensslin, D.C. Driscoll, A.C. Gossard, Appl. Phys. Lett. 85 (2004) 2005.
[25] L.M.K. Vandersypen, J.M. Elzerman, R.N. Schouten, L.H. Willems van Beveren, R. Hanson, L.P. Kouwenhoven, Appl. Phys. Lett. 85 (2004) 4394.
[26] S. Gustavsson, R. Leturcq, B. Simovic, R. Schleser, T. Ihn, P. Studerus, K. Ensslin, D.C. Driscoll, A.C. Gossard, Phys. Rev. Lett. 96 (2006) 076605.
[27] S. Gustavsson, R. Leturcq, T. Ihn, K. Ensslin, M. Reinwald, W. Wegscheider, Phys. Rev. B 75 (2007) 075314.
[28] T. Fujisawa, T. Hayashi, R. Tomita, Y. Hirayama, Science 312 (2006) 1634.
[29] A. Fuhrer, A. Dorn, S. Lüscher, T. Heinzel, K. Ensslin, W. Wegscheider, M. Bichler, Superlattice Microstructure 31 (2002) 19.
[30] O. Naaman, J. Aumentado, Phys. Rev. Lett. 96 (2006) 100201.
[31] C.E. Shannon, Proc. Institute of Radio Engineers 37 (1949) 10.
[32] D.A. Bagrets, Y.V. Nazarov, Phys. Rev. B 67 (2003) 085316.
[33] L.P. Kouwenhoven, C.M. Marcus, P.M. McEuen, S. Tarucha, R. M. Westervelt, N.S. Wingreen, in: L.L. Sohn, L.P. Kouwenhoven, G. Schön (Eds.), Mesoscopic Electron Transport, NATO ASI Series E, vol. 345, Kluwer Academic Publishers, Dordrecht, 1997, pp. 105–214.